Title

Restriction spectrum imaging reveals decreased neurite density in patients with temporal lobe epilepsy

Journal

Epilepsia, 57(11)

ISSN

0013-9580

Authors

Loi, Richard Q
Leyden, Kelly M
Balachandra, Akshara
et al.

Publication Date

2016-11-01

DOI

10.1111/epi.13570

Peer reviewed

FULL-LENGTH ORIGINAL RESEARCH

Restriction spectrum imaging reveals decreased neurite density in patients with temporal lobe epilepsy

*Richard Q. Loi, *Kelly M. Leyden, *Akshara Balachandra, *Vedang Uttarwar, *†Donald J. Hagler Jr, ‡§Brianna M. Paul, *†Anders M. Dale, *†Nathan S. White, and *¶Carrie R. McDonald

Epilepsia, 57(11):1897–1906, 2016
doi: 10.1111/epi.13570

Richard Q. Loi is a UC San Diego masters graduate and a medical student at Wayne State School of Medicine, U.S.A.

Summary

Objective: **Diffusion tensor imaging (DTI) has become a popular tool for delineating the location and extent of white matter injury in temporal lobe epilepsy (TLE). However, DTI yields nonspecific measures that are confounded by changes occurring within both the intracellular and extracellular environments. This study investigated whether an advanced diffusion method, restriction spectrum imaging (RSI) could provide a more robust measure of white matter injury in TLE relative to DTI due to RSI's ability to separate intraaxonal diffusion (i.e., neurite density; ND) from diffusion associated with extraaxonal factors (e.g., inflammation; crossing fibers).**

Methods: **RSI and DTI scans were obtained on 21 patients with TLE and 11 age-matched controls. RSI-derived maps of ND, isotropic-hindered (IH) and isotropic-free (IF) water, and crossing fibers (CFs) were compared to DTI-derived fractional anisotropy (FA) maps. Voxelwise and tract-based analyses were performed comparing patients with TLE to controls on each diffusion metric.**

Results: **Reductions in FA were seen primarily in frontotemporal white matter in TLE, and they were most pronounced proximal to the seizure focus. Reductions in ND corresponded to those seen in the FA maps; however, ND reductions were greater in magnitude, more lateralized to the epileptogenic hemisphere, and showed a broader pattern. Increases in IF/IH and effects from CFs also contributed to reduced FA in the ipsilateral parahippocampal cingulum and fornix, with decreases in IH extending into extratemporal regions. Reduced ND of the uncinate fasciculus was associated with longer disease duration, whereas FA was not associated with any clinical variables.**

Significance: **RSI may provide a more specific measure of white matter pathology in TLE, distinguishing regions primarily affected by axonal/myelin loss from those where CFs and increases in extracellular water also play a role. By providing a more specific measure of axonal/myelin loss, RSI-derived ND may better reflect overall white matter burden in epilepsy.**

KEY WORDS: **Diffusion tensor imaging, Intracellular diffusion, Fractional anisotropy, Crossing fibers, Restricted diffusion.**

Temporal lobe epilepsy (TLE) is the most common localization-related epilepsy and may be highly refractory to medication management.[1] Although once considered to be a disease of the hippocampus, it is now well appreciated that TLE is a network disorder associated with damage to multiple cortical and subcortical structures that extend well beyond the medial temporal lobes.[2,3] In fact, studies using diffusion tensor imaging (DTI) have consistently revealed bilateral patterns of microstructural damage to multiple

Accepted August 29, 2016; Early View publication 13 October 2016.
*Multimodal Imaging Laboratory, University of California, San Diego, La Jolla, California, U.S.A.; †Department of Radiology, University of California, San Diego, La Jolla, California, U.S.A.; ‡Department of Neurology, University of California, San Francisco, California, U.S.A.; §UCSF Comprehensive Epilepsy Center, University of California, San Francisco, California, U.S.A.; and ¶Department of Psychiatry, University of California, San Diego, La Jolla, CA, U.S.A.

Address correspondence to Carrie McDonald, Multimodal Imaging Laboratory, University of California, 8950 Villa La Jolla Dr, Suite C101, La Jolla, CA 92037, U.S.A. E-mail: camcdonald@ucsd.edu

Wiley Periodicals, Inc.

Key Points

- RSI is an advanced, multicompartment diffusion model that separates intracellular from extracellular diffusion and can model complex fiber orientation and structure
- RSI-derived "neurite density" (ND) shows a more robust and lateralized pattern of white matter compromise in TLE compared to DTI-derived FA
- Reduced ND, but not FA, of the uncinate fasciculus is associated with longer disease duration in TLE
- RSI-derived ND may provide a more sensitive and specific measure of white matter compromise in TLE compared to FA by more precisely estimating axonal and/or myelin loss

long-range association tracts, with greater compromise to fiber tracts ipsilateral and proximal to the seizure focus.[3–5] This is typically demonstrated by decreases in fractional anisotropy (FA) and/or increases in mean diffusivity (MD) along entire fiber tracts or within subsections of a tract, which are interpreted as reflecting axonal loss and demyelination of white matter within the affected regions.

Despite the unique insights obtained from traditional DTI, it is increasingly appreciated that FA and MD are nonspecific measures of cerebral pathology that are influenced by a number of tissue-related factors.[6] In addition to axonal loss and demyelination, decreases in FA obtained from the basic tensor model may reflect the presence of crossing fibers or increases in extracellular diffusion due to edema or inflammation.[7,8] Given recent data suggesting that inflammation may play a role in the pathogenesis of TLE,[9] better understanding of the neurobiology of decreased FA in temporal and extratemporal regions could help to guide treatments in patients with TLE or other epilepsy syndromes.[9]

In recent years, a number of advanced diffusion methods have emerged that extend beyond the tensor model and may provide more sensitive and/or specific measures of cerebral pathology in TLE.[6,10–13] Diffusion kurtosis imaging (DKI), which is a statistical method that probes non-Gaussian diffusion and estimates diffusion heterogeneity,[14] has been applied in several studies of children[12] and adults[10,11] with TLE. These studies have suggested that kurtosis measures reveal a broader and more robust pattern of microstructural abnormalities in TLE compared to conventional DTI, which may reflect the greater sensitivity of DKI to multiple pathologic factors including cell loss, inflammation, and axonal and dendritic reorganization. In addition, diffusion spectrum imaging (DSI), a high-angular diffusion imaging (HARDI) technique, has recently been combined with a multicompartment diffusion model, the neurite orientation dispersion and density imaging (NODDI) model, to estimate structural connectivity and network properties in TLE.[13] This DSI study revealed that reduced FA in the medial temporal lobes was driven primarily by reductions in intracellular diffusion, commensurate with neurite loss (i.e., cell and axonal or myelin loss), whereas reduced FA in extratemporal regions was also driven by fiber orientation changes (i.e., high orientation dispersion index; ODI), potentially reflecting disorganized fiber orientation and packing. These studies suggest that advanced diffusion techniques, which aim to resolve intravoxel tissue properties, may provide more sensitive measures of network pathology in TLE.

In this study, we apply a new multicompartment diffusion model, restriction spectrum imaging (RSI), which combines key properties of these existing methods to resolve whether decreases in FA in patients with TLE are better explained by decreased axonal/neurite density (ND), crossing fibers (CF), and/or increases in extracellular diffusion (i.e., isotropic-hindered [IH] and isotropic-free [IF] water diffusion).[15] This new method is an extension of traditional HARDI techniques for reconstructing CFs and modeling complex orientation and structure, but within a clinically feasible scan frame (4–8 min). Using multiple diffusion weightings (b-values), RSI further distinguishes hindered and restricted diffusion pools in the extracellular and intracellular compartments, respectively, and models both spherically restricted (within cells) and cylindrically restricted (within axons) diffusion (see Fig. 1). Isolating the anisotropic, restricted compartment within axons is important, as this allows for estimates of the axonal density and orientation distribution that are distinct from changes in extracellular diffusion. Thus, the ability of RSI to probe both the scale and geometry of tissue microstructure, positions it well to determine whether regional reductions in DTI-derived FA values are due to axonal loss/demyelination versus extracellular changes (e.g., cerebrospinal fluid [CSF]–filled spaces; inflammation) or CFs. We have shown previously the advantage of RSI over standard DTI for reconstructing fiber tracts in regions of peritumoral edema,[8] identifying regions of high cellularity in patients with high-grade glioma,[16] and evaluating response to therapy in patients treated with bevacizumab.[17] We now extend the application of RSI to unveiling the complex cytoarchitecture of white matter injury in patients with TLE.

Materials and Methods

Participants

This study was approved by the University of California, San Diego (UCSD) Institutional Review Board, and all participants provided informed consent according to the Declaration of Helsinki. Twenty-one patients with medically refractory TLE and 11 age-matched controls had volumetric magnetic resonance imaging (MRI), DTI/RSI, and clinical data that allowed for inclusion in the study. All patients were under evaluation for surgical treatment at the UCSD Epilepsy Center. They were diagnosed with medically refractory epilepsy by board-certified neurologists with

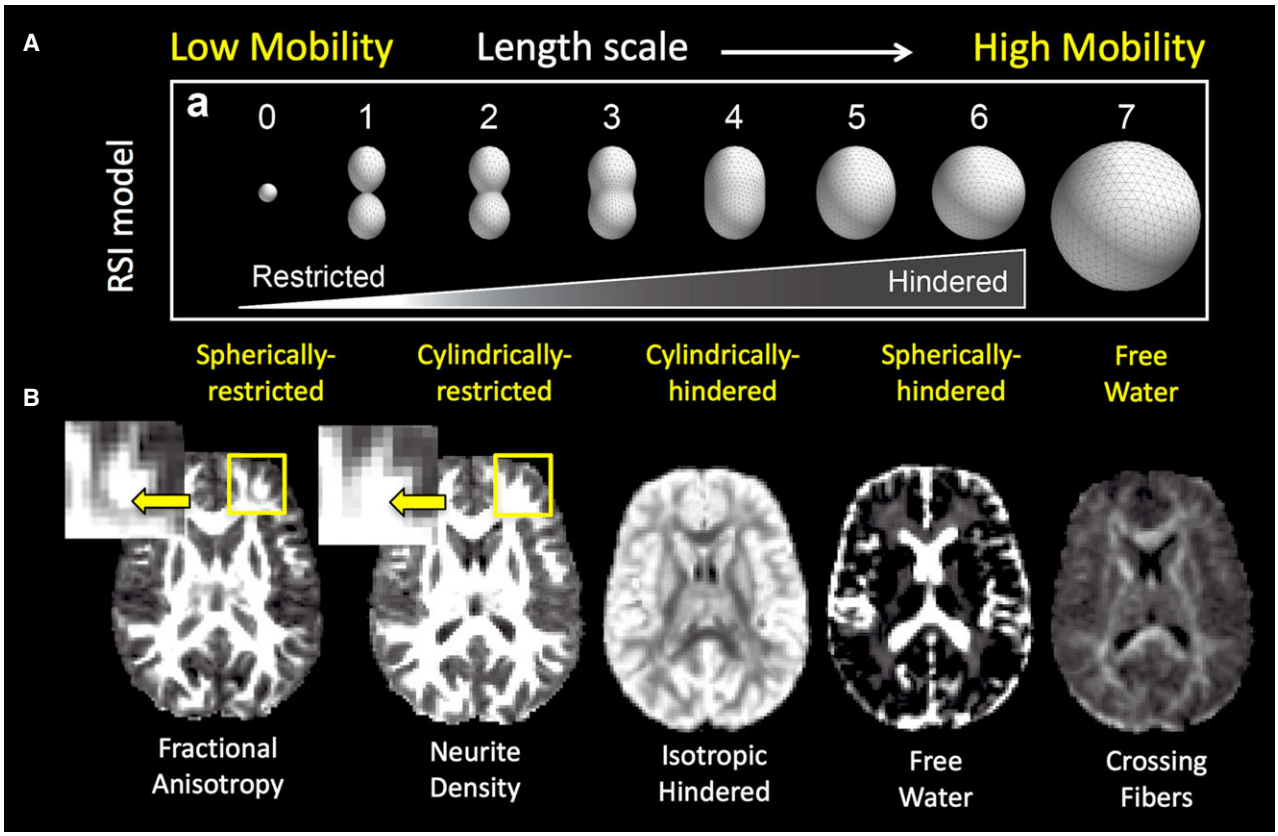

Figure 1.
(**A**) Illustration of the full RSI "spectrum." This model takes into account both the size scale and geometry of diffusion, separating free, hindered, and restricted water compartments within a voxel. The model in this article included the following components: cylindrically restricted (ND), crossing fiber (CF), and both isotropic-hindered (IH) and isotropic-free (IF) water compartments. (**B**) Axial slice of fractional anisotropy (FA), ND, IH, IF, and CF maps. Insets illustrate a region in which crossing fibers reduce FA, but ND is not affected.

expertise in epileptology, according to the criteria defined by the International League Against Epilepsy (ILAE). Patients were classified as left TLE (LTLE; n = 10) or right TLE (RTLE; n = 11) based on seizure onsets recorded by video–electroencephalography (EEG), seizure semiology, and neuroimaging results. Clinical MRI scans were available on all patients (i.e., T_1-weighted, T_2-weighted, and coronal fluid-attenuated inversion recovery [FLAIR] sequences with 1-mm slices through the mesial temporal lobe). MRI studies were visually inspected by a board-certified neuroradiologist for detection of mesial temporal sclerosis (MTS) and the exclusion of contralateral temporal lobe structural abnormalities. In eight patients, MRI findings suggested the presence of ipsilateral MTS. No patients showed evidence of contralateral MTS or extrahippocampal pathology on clinical MRI. Control participants were screened for neurologic or psychiatric conditions.

MRI acquisition

All patients were seizure-free per self-report for a minimum of 24 h prior to the MRI scan. All brain imaging was performed on a General Electric Discovery MR750 3T scanner with an 8-channel phased-array head coil. Image acquisition included a conventional three-plane localizer, GE calibration scan, a T_1-weighted three-dimensional (3D) structural scan (repetition time [TR] = 8.08 msec, echo time [TE] = 3.16 msec, inversion time [TI] = 600 msec, flip angle = 8 degrees, field of view [FOV] = 256 mm, matrix = 256 × 192, slice thickness = 1.2 mm), and for diffusion MRI, a single-shot pulsed-field gradient spin-echo echo planar imaging (EPI) sequence (TE/TR = 96 msec/17 s; FOV = 24 cm, matrix = 128 × 128 × 48; axial; 2.5 mm isotropic resolution, resampled to 1.875 mm isotropic). Diffusion data used for the standard DTI analysis were acquired with b-value = 0 and 1,000 mm^2/s with 30 unique gradient directions. Diffusion data used for the RSI analyses were acquired with b = 0, 500, 1,500, and 4,000 s/mm^2, with 1, 6, 6, and 15 unique gradient directions for each b-value, respectively (total RSI scan time = ~5 min). These parameters were selected to optimize statistical efficiency, based on simulations described in White and Dale.[18,19] For use in nonlinear B0 distortion correction, two additional b = 0 volumes were acquired with either forward or reverse phase-encode polarity.

DTI and RSI processing

Preprocessing of the diffusion data included correction for B0 distortion, eddy current distortions, gradient nonlinearity distortions, and head motion, as well as registration to the T_1-weighted structural image. For B0 distortion correction, a reverse gradient method was used.[20] This method provides superior accuracy and better cross-modality registration relative to the field mapping approach. A detailed description of the image processing is provided elsewhere.[21]

DTI-derived FA and MD were calculated based on a tensor fit to the b = 1,000 data. Conversely, RSI utilizes a multi-b-shell acquisition in conjunction with a linear mixture model to isolate diffusion signals from separable hindered, restricted, and free water diffusion compartments within a voxel. Technical details describing the RSI mathematical framework are described in full elsewhere.[15,16,22] RSI-based measures of ND, CF, IH, and IF were calculated from the estimated volume fraction of the 2nd and 4th order spherical harmonics of the cylindrically restricted (ND) compartment, the 4th order spherical harmonic component of the cylindrically restricted compartment (CF), and the IH, and IF water compartments, respectively. All measures were normalized to the squared sum of squares of all model coefficients. The RSI model was fit to the data using least-squares estimation with Tikhonov regularization.[16]

Whole brain map processing

Voxel-based analysis

Voxel-based analysis (VBA) was conducted according to the ANTS-Groupwise processing pipeline—a modified Tract-Based Spatial Statistics (TBSS; http://fsl.fmrib.ox.ac.uk/fsl/fslwiki/TBSS) processing pipeline described by Schwarz et al.[23] that has been shown to be more sensitive for detecting changes and to have greater specificity in resisting false positives from misregistration relative to the existing pipeline. Individual T_1-weighted images were iteratively registered to form a groupwise map using the Advanced Normalization Tools-Symmetric Normalization (ANTS-SyN) ver-1.9.4 algorithm.[24] Groupwise T_1-weighted templates were formed for LTLE and RTLE combined with controls through the ANTS toolbox. Individual T_1 warps to the groupwise template were applied to individual whole-brain diffusion maps to better register maps by avoiding logical circularity in intrameasure registrations.[25] The diffusion maps were further binarized with white matter masks generated by the Oxford Centre for Functional MRI of the Brain's (FMRIB) Automated Segmentation Tool (FAST) using individual registered T_1-weighted images, and voxels were included only if nonzero in ≥70% of the co-registered subjects.[23] Each DTI or RSI-derived diffusion map was smoothed with a 5-mm full-width at half-maximum Gaussian kernel. Statistical comparisons were performed with a general linear model design of a two independent sample *t*-test with 5,000 permutations run on FSL's Randomize that identified voxelwise differences between each patient group and healthy controls. Voxelwise analysis utilized Threshold-Free Cluster Enhancement (TFCE) with 3D voxel optimization to enhance clustering.[26] All VBA maps were corrected for multiple comparisons using a false discovery rate (FDR) threshold of $q < 0.05$.

Fiber tract calculations

Fiber tract values for each of the DTI and RSI diffusion measures were derived using a probabilistic diffusion tensor atlas that was developed using in-house software written in Matlab and C++ (i.e., AtlasTrack). A full description of the atlas and the steps used to create the atlas are described elsewhere.[27] For each participant, T_1-weighted images were used to nonlinearly register the brain to a common space, and diffusion tensor orientation estimates were compared to the atlas to obtain a map of the relative probability that a voxel belongs to a particular fiber given the location and similarity of diffusion orientations. Voxels identified with FreeSurfer's automated brain segmentation as CSF or gray matter were excluded from the fiber regions of interest (ROIs). Average diffusion metrics were calculated for each fiber ROI, weighted by fiber probability, so that voxels with low probability of belonging to a given fiber contributed minimally to average values. In the current study, this probabilistic atlas-based method was used to reconstruct the following right and left hemisphere fiber tracts due to evidence of their disruption in TLE[2]: fornix (FX), parahippocampal cingulum (PHC), dorsal cingulum bundle (CING), uncinate fasciculus (UNC), inferior longitudinal fasciculus (ILF), and the inferior frontal occipital fasciculus (IFOF) (see Fig. 2).

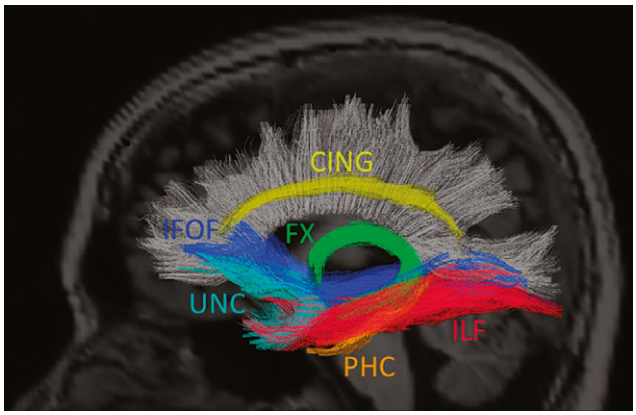

Figure 2.
Sagittal rendering of six fiber tracts of interest in this study derived using a probabilistic diffusion tensor atlas (i.e., AtlasTrack) and projected onto a T_1-weighted image. CING, dorsal cingulum; PHC, parahippocampal cingulum; FX, fornix; UNC, uncinate fasciculus; IFOF, inferior frontal occipital fasciculus; ILF, inferior longitudinal fasciculus.

Structural MRI processing

T_1-weighted images were corrected for nonlinear warping caused by nonuniform fields created by the gradient coils. Image intensities were corrected for spatial sensitivity inhomogeneities in the 8-channel head coil by normalizing with the ratio of a body coil scan to a head coil scan. Hippocampal volumes were obtained using FreeSurfer's subcortical segmentation pipeline and individually checked for accuracy by an expert anatomist and image analyst.

Statistical analysis

Analyses of variance (ANOVAs) and independent *t*-tests were used to test for differences among the groups in key demographic and clinical variables. Whole-brain VBA, comparing patients with LTLE and RTLE separately to controls, was performed for DTI (FA and MD) and RSI (ND, CF, IH, and IF) metrics using voxelwise *t*-tests. Tract-based ROI analyses were also performed between each patient group's ipsilateral and contralateral fiber tracts and those of controls for each fiber tract using *t*-tests. Pearson correlations were used to examine relationships between our diffusion measures and clinical variables (i.e., age of seizure onset, disease duration, and seizure frequency). For fiber ROI analysis, a Bonferroni-corrected p-value of $p < 0.00416$ was used to correct for multiple comparisons.

Results

Table 1 displays demographic and clinical variables for the patient and control groups. There were no statistically significant differences among the controls, LTLEs, or RTLEs in age ($F[2,29] = 0.634$, $p > 0.05$). However, there was a group difference in years of education ($F[2,29] = 4.02$, $p < 0.05$), with controls achieving a higher level of education than either patient group. The distribution of gender across the three groups was comparable ($\chi^2[2] = 1.90$, $p > 0.05$). There were no statistically significant differences between the two patient groups in disease duration ($t[17] = 1.63$, $p > 0.05$), age at seizure onset ($t[17] = -0.77$, $p > 0.05$), seizure frequency ($t[17] = 0.47$, $p > 0.05$), or the number of patients with MTS ($\chi^2[1] = 1.56$, $p > 0.05$). However, the volume of the ipsilateral hippocampus was slightly smaller in patients with LTLE compared to those with RTLE ($t[19] = -2.44$, $p = 0.025$). Contralateral hippocampal volumes (HCVs) did not differ between the patient groups ($t[19] = 0.51$, $p > 0.05$). Ipsilateral HSVs in both patient groups were smaller when compared to HCVs on the corresponding side for the controls ($t[19] = 4.09$, $p = 0.001$, and $t[20] = 2.50$, $p = 0.04$, LTLE and RTLE, respectively), but their contralateral HCVs were not statistically different from the controls ($t[19] = 0.508$, $p > 0.05$, and $t[20] = 0.93$, $p > 0.05$, LTLE and RTLE, respectively).

VBA analysis

Figure 3 reveals voxelwise maps of significant decreases in FA and ND and increases in MD and IF in each patient group compared to controls. Suprathreshold effects were minimal in the IH VBA maps and largely overlapped with IF. As can be seen, patients with LTLE showed decreased FA primarily in the left anterior temporal lobe, with additional regions of decreased FA in the inferior prefrontal and retrosplenial white matter. Increases in MD were more restricted, with few exceeding using a false discovery rate (FDR; http://fsl.fmrib.ox.ac.uk/fsl/fslwiki/FDR) threshold. Compared to FA, ND maps revealed a broader and more robust pattern of decreases in LTLE, with strong lateralization to the left hemisphere. In addition, small areas of increased IF are observed in left temporal lobe regions in and around regions of decreased ND.

In patients with RTLE, there were few regions in which decreased FA or MD survived our FDR correction in the voxelwise analysis. However, a more lenient threshold ($p < 0.02$) showed strong trends in the data of decreased FA and increased MD that follow the same pattern observed in LTLE (see Fig. S1). Similar to the pattern seen in LTLE, ND maps in RTLE revealed a broad and robust pattern of ND decreases, with strong lateralization to the right anterior temporal and prefrontal region. Minimal increases in IF were noted. There were no suprathreshold differences in CF between controls and patients with LTLE or RTLE in the voxelwise analysis.

Table 1. Demographic and clinical characteristics of the participants

	Control (n = 11)	LTLE (n = 10)	RTLE (n = 11)
Age	37.79 (17.94)	43.50 (12.07)	38.09 (12.88)
Gender	8 M, 3 F	5 M, 5 F	5 M, 6 F
Education (years)	16.91 (2.77)	14.40 (1.65)	14.60 (2.37)
Age of onset (years)	N/A	15.40 (19.24)	21.65 (16.72)
Duration (years)	N/A	28.20 (16.36)	17.65 (15.04)
MTS status	N/A	5+, 5−	3+, 8−
Seizure frequency (# per month)	N/A	10.70 (17.38)	6.12 (12.93)
Left hippocampal volume (mm^3)	4,089.85 (396.85)	2,843.76 (922.66)	3,871.69 (669.41)
Right hippocampal volume (mm^3)	4,115.62 (595.79)	3,998.87 (434.87)	3,699.19 (679.07)

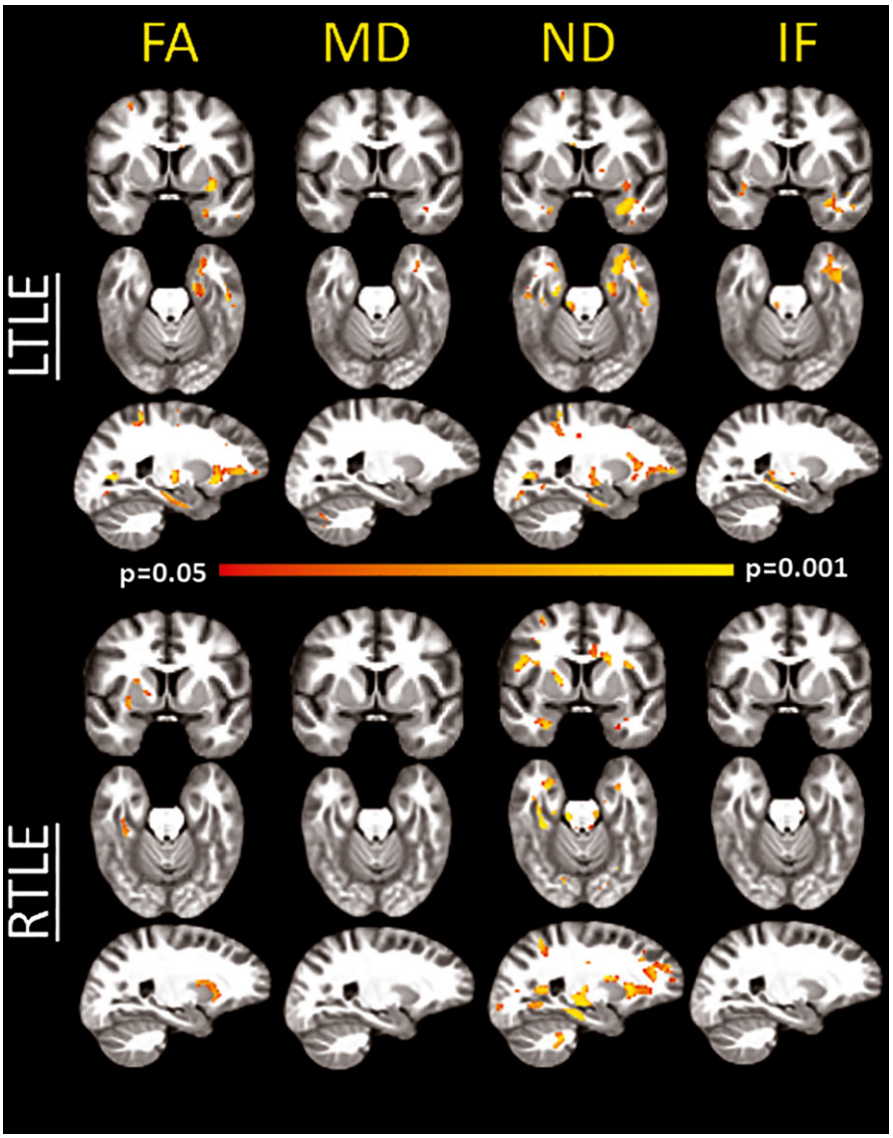

Figure 3.
Voxel-based analysis group comparisons between patients with right TLE (RTLE) or left TLE (LTLE) and age-matched controls using ANTS registration. Areas of red-yellow represent decreased FA and ND and increased MD and IF in patients compared to controls. All images are clustered and FDR-corrected at $q < 0.05$.
Epilepsia © ILAE

Tract-based analysis

Because patients with LTLE and RTLE showed a similar pattern of reductions in FA and ND that differed mostly in magnitude (i.e., LTLE showed more pronounced reduction in FA relative to RTLE), we combined the patient groups to examine diffusion parameters in ipsilateral and contralateral fiber tracts (see Table 2). Patients with TLE showed ipsilateral and contralateral reductions in FA and ND in the FX, CING, PHC, UNC, and ILF. In addition, ND only was reduced in the ipsilateral IFOF. Complementing our voxelwise analysis, the magnitude of the effects was consistently larger with ND than with FA (Cohen's d), particularly in the contralateral UNC and ipsilateral IFOF where effect sizes for ND were 33% and 66% higher, respectively. In addition, increases in IF and MD were observed in the ipsilateral FX ($t[30] = -3.5$, $p = 0.001$ for IF; $t[30] = -3.0$, $p = 0.004$ for MD) and PHC ($t[30] = -3.3$, $p = 0.002$ for IF; $t[30] = -2.9$, $p = 0.001$ for MD) in patients compared to controls. Increases in IH were also observed in the ipsilateral FX ($t[30] = 3.3$, $p = 0.002$), ipsilateral CING ($t[30] = 3.3$, $p = 0.002$), and bilateral PHC ($t[30] = 4.1$, $p = 0.0003$ for ipsilateral; $t[30] = 3.3$, $p = 0.002$ for contralateral). There was also a strong trend toward increased IH in the ipsilateral UNC ($t[30] = 2.9$, $p = 0.007$). The effects of CFs were also greater in controls in the ipsilateral FX ($t[30] = 3.1$, $p = 0.002$ and PHC $t[30] = 3.3$, $p = 0.003$), suggesting more complex fiber structure in controls Mean volume fractions and raw values for IF, IH, MD, and CF in each fiber tract ROI are provided in the Supporting Information Tables S1 and S2.

Correlation with clinical variables

Lower ND in the ipsilateral UNC was strongly associated with a longer disease duration ($r = 0.66$; $p = 0.003$), whereas there were no significant correlations between FA,

Table 2. FA and ND of the ipsilateral and contralateral fiber tracts for controls and patients with TLE

	Controls Mean	TLEs Mean	T-Score	p-Value	Cohen's d
FX					
Ipsilateral[a,b]					
FA	0.3030 (0.02137)	0.2353 (0.05535)	3.884	0.000524	1.6136
ND	0.4354 (0.02860)	0.3011 (0.09440)	4.577	0.000077	1.9255
Contralateral					
FA	0.3030 (0.02137)	0.2481 (0.05081)	3.412	0.001866	1.4085
ND	0.4354 (0.02860)	0.3269 (0.08955)	3.890	0.000516	1.6322
CING					
Ipsilateral[b]					
FA	0.4719 (0.01929)	0.4101 (0.04546)	4.285	0.000173	1.7697
ND	0.6698 (0.02674)	0.5799 (0.04676)	5.869	0.000002	2.3602
Contralateral					
FA	0.4719 (0.01929)	0.4164 (0.04882)	3.601	0.001128	1.6649
ND	0.6698 (0.02674)	0.5963 (0.05194)	4.379	0.000134	1.7792
PHC					
Ipsilateral[a,b]					
FA	0.3434 (0.04255)	0.2163 (0.09259)	4.286	0.000183	1.7639
ND	0.4828 (0.07161)	0.3012 (0.10740)	5.011	0.000025	1.9895
Contralateral[b]					
FA	0.3434 (0.04255)	0.2397 (0.10456)	3.136	0.003813	1.2991
ND	0.4828 (0.07161)	0.3342 (0.11078)	4.016	0.000366	1.5931
UNC					
Ipsilateral					
FA	0.4473 (0.03507)	0.3839 (0.05778)	3.302	0.002553	1.3265
ND	0.6319 (0.03244)	0.5679 (0.07125)	2.809	0.003796	1.1561
Contralateral					
FA	0.4473 (0.03507)	0.4180 (0.03775)	2.119	0.042812	0.8041
ND	0.6319 (0.03244)	0.5940 (0.03041)	3.246	0.002948	1.2054
ILF					
Ipsilateral					
FA	0.4733 (0.02371)	0.4441 (0.04467)	2.014	0.053091	0.8165
ND	0.6773 (0.01661)	0.6379 (0.05623)	2.255	0.031604	0.9503
Contralateral					
FA	0.4733 (0.02371)	0.4569 (0.04080)	1.224	0.230354	0.4914
ND	0.6773 (0.01661)	0.6490 (0.04381)	2.055	0.048681	0.8542
IFOF					
Ipsilateral					
FA	0.4885 (0.02485)	0.4733 (0.03149)	2.774	0.009435	0.5358
ND	0.6854 (0.02462)	0.6394 (0.03284)	4.066	0.000318	1.5849
Contralateral					
FA	0.4885 (0.02485)	0.4793 (0.03340)	0.806	0.426731	0.3125
ND	0.6854 (0.02462)	0.6600 (0.03867)	1.968	0.058393	0.7835

[a]Fiber tracts that demonstrate a significant difference ($p < 0.00416$) in CF, MD, and IF between controls and TLEs.
[b]Fiber tracts that demonstrate a significant difference ($p < 0.00416$) in IH between controls and TLEs.

MD, CF, or IF and any of the clinical variables in our patient cohort.

Discussion

In this study, we demonstrate the value of a new advanced diffusion imaging technique, RSI, for better elucidating the nature of white matter injury in patients with TLE compared to traditional DTI. The advantage of RSI in this scenario stems from its ability to separate intracellular from extracellular diffusion while simultaneously modeling complex fiber structure (i.e., CFs). This ability to probe both the scale and geometry of tissue microstructure likely allows for a more precise estimate of axonal and/or myelin loss. In a group of patients with refractory TLE, we found reductions in ND that generally corresponded to decreases in FA. However, decreases in ND were greater in magnitude and showed a broader pattern of decreases compared to FA. This finding was demonstrated in both our voxelwise and tract-based analysis and is commensurate with a small, but growing literature demonstrating improved sensitivity of advanced diffusion imaging for delineating white matter pathology in epilepsy. Similar to studies indicating that DKI-derived measures (e.g., mean kurtosis) may provide a

more sensitive measure of pathology,[10,12,28–30] we found the pattern of reduced ND to be more robust and congruent with known network abnormalities in TLE, which are most prominent within medial temporal/limbic networks ipsilateral and proximal to the seizure focus[5] (Fig. 3). However, it is important to note that whereas reduced kurtosis indicates a loss of diffusion heterogeneity—a metric that should correlate with a loss of diffusion restriction, and therefore, white matter pathology—RSI is a multicompartment model that can more directly probe the nature of this pathology. That is, RSI quantifies the degree to which diffusional heterogeneity within a voxel is driven by decreases in intraaxonal water (i.e., loss of ND) versus increases in extracellular diffusion (i.e., increased IF and IH) while accounting for complex fiber orientation. Thus, similar to DSI with NODDI, RSI provides a biophysical model for separating different tissue compartments and modeling the geometry of the neurite compartment. However, RSI takes this one step further by also characterizing CFs and volume fractions of fibers in multiple directions. Whereas the ODI obtained from NODDI provides a single estimate of the dispersion of fibers within a voxel, RSI can further characterize the nature of dispersion (i.e., whether high dispersion reflects crossing fibers or just fanned out fibers), and within a clinically feasible time frame (i.e., DSI typically takes ~30 min to acquire compared to ~4–7 min for RSI).

The increased precision of this measure may be reflected by the fact that decreased ND, but not FA, was associated with longer disease duration in our patient cohort in the UNC. This association is particularly interesting given the proposed role of the UNC in seizure propagation[31] as well as the vulnerability of this white matter tract in TLE.[32] Whether loss of neurites in the UNC is due to years of refractory seizures versus other treatment- or disease-related factors requires testing in longitudinal series. We propose that RSI-derived ND could provide a better means for capturing these changes than current DTI-based metrics.

In addition to our main finding of significant reductions in ND, increases in IF were found proximal to the epileptic focus in both the ipsilateral FX and PHC, whereas increases in IH extended into the ipsilateral CING and contralateral PHC in the fiber ROI analysis. In general, IF and IH appeared to be highly related in TLE, but with additional extratemporal increases seen for IH. However, increases in extracellular water did not appear to be a dominant source of pathology in the other fiber tracts. Increases in the hindered and free water fractions may reflect a number of pathologic processes, including increased CSF in spaces surrounding axon/myelin loss and/or local tissue inflammation. The former is a more simplistic explanation and one that is supported by analysis of excised fornix tissue scanned at 7T.[33] However, surgical specimens from patients with TLE also suggest an increase in inflammatory infiltrates in excised temporal lobe tissue,[34] and recent positron emission tomography (PET) studies have shown increases in biomarkers of inflammation (i.e., translocator protein; TSPO) in the bilateral temporal lobes in TLE,[35] suggesting ongoing local inflammation in patients with refractory seizures. Studies using advanced diffusion imaging in patients with multiple sclerosis[36] and schizophrenia[7] have recently linked an increase in the isotropic restricted and isotropic free water compartments, respectively, to neuroinflammation. However, histologic validation of these in vivo diffusion metrics is based primarily on preclinical data,[37] whereas validation in humans is still limited (but see Wang et al.[36]). Although we are not able to provide unique biologic explanations for increased IH versus IF in this study, future work with RSI will address whether these extracellular components can differentiate local tissue inflammation/edema from CSF-filled pockets, respectively.

We also found group differences in CFs in both the ipsilateral FX and PHC. The greater effect of CFs in these regions likely reflects a more complex fiber structure in controls (see Fig. 4). CFs are ubiquitous in the brain and it is well known that they contribute to FA decreases in some regions more than others. In the medial temporal lobe, the PHC is crossed by fibers of the perforant path and adjacent pathways, which run from the entorhinal cortex into the hippocampus[38] and are known to be affected in TLE.[39] Figure 4 shows a voxel taken from the PHC in a patient and control. As can be seen, FA is lower in the control (i.e., represented by a more spherical tensor) due to the presence of CFs in this region, whereas FA is not reduced in the patient due to simplified fiber structure. Although the reason for this simplified fiber structure in TLE is unknown, it is possible that the dying off of perpendicular axons within the

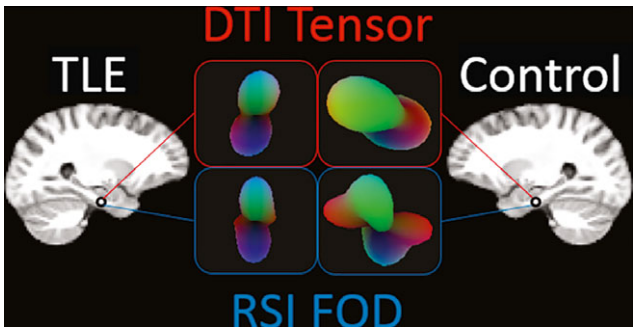

Figure 4.
Example of a DTI-derived tensor and an RSI-derived fiber orientation distribution (FOD) from a voxel within the right PHC of a patient with RTLE and a control. As can be seen, the FOD reveals a more complex fiber orientation in the control (i.e., crossing fibers) that is not revealed in the DTI tensor. Conversely, the tensor and FOD appear similar in the patient due to a lack of crossing fibers, potentially due to axonal loss in fiber bundles perpendicular to the PHC.
Epilepsia © ILAE

perforant path and adjacent fibers bundles leads to this simplified structure in patients, driving up FA values in the PHC in patients more so than in controls. Like HARDI models, RSI can model this complex fiber structure, producing measures of ND and IH/IF fractions that are not affected by CFs.

Our study demonstrates the utility of RSI for delineating the nature of white matter pathology in TLE. Other strengths of our study include an analysis of white matter microstructure at both the voxelwise and tract-based levels, and our use of an advanced image registration method (i.e., ANTS) that has been shown to be robust for groupwise diffusion-based analysis.[23] However, there are several limitations to our study that should be noted. First, the sample size is relatively small, and we may not have had the power to detect subtle group differences in some fiber tracts that may be revealed with a larger cohort. However, it is important to note that we were able to capture many robust associations with ND with large effects sizes even in a small cohort. This could translate to needing fewer patients enrolled in clinical trials to demonstrate an effect when RSI- versus DTI-derived metrics are used. Second, we included patients with and without MTS in the same analysis. There is now considerable evidence that DTI-derived abnormalities are more pronounced in patients with radiologic evidence of MTS.[2,40] In our small sample, it is of note that patients with MTS demonstrated a trend toward lower ND in the PHC relative to those without MTS ($p = 0.054$), and this likely contributed to the stronger patterns in FA and ND loss seen in the VBA maps in LTLE (the group with a greater number of patients with MTS) relative to RTLE. However, our group of MTS+ ($N = 8$) and MTS- ($N = 13$) were too small and unbalanced to analyze separately in this initial study. Future research with a larger patient sample will test the utility of RSI-derived measures in each patient cohort separately. Although the RSI acquisition scheme was selected to optimize scanning and statistical efficiency, the number of parameters estimated is on the cusp given the available data. Additional information may be gleaned from collecting more data. However, this would result in a longer scan time, likely decreasing its clinical feasibility without significantly improving the signal to noise.[18,19] Finally, although we believe that our multicompartment diffusion model offers advantages over many existing models for better elucidating the nature of white matter changes within a clinically feasible time frame, as with most diffusion techniques, histologic validation of the RSI-model is primarily limited to preclinical data[15] and will require further validation in patients with TLE. As numerous promising advanced diffusion techniques are now emerging, there is also a significant need to directly compare these techniques to one another and to determine which method(s) provides the most clinically meaningful information for patients with TLE and other epilepsy syndromes.

Acknowledgments

We wish to thank Holly M. Girard for assistance in data collection. We also wish to thank the patients of the UCSD Epilepsy Center who devoted their time and clinical data for research purposes.

Funding

This work was supported by the National Institutes of Health (NIH)/National Institute of Neurological Disorders and Stroke (NINDS; R01NS065838 to CRM). The NIH had no role in the study design; in the collection, analysis, and interpretation of data; in the writing of the report; or in the decision to submit the article for publication.

Disclosure

None of the authors listed on this manuscript has a conflict of interest to disclose. We confirm that we have read the Journal's position on issues involved in ethical publication and affirm that this report is consistent with those guidelines.

References

1. Engel J Jr, Wiebe S, French J, et al. Practice parameter: temporal lobe and localized neocortical resections for epilepsy. *Epilepsia* 2003;44:741–751.
2. Rodriguez-Cruces R, Concha L. White matter in temporal lobe epilepsy: clinico-pathological correlates of water diffusion abnormalities. *Quant Imaging Med Surg* 2015;5:264–278.
3. Ahmadi ME, Hagler DJ Jr, McDonald CR, et al. Side matters: diffusion tensor imaging tractography in left and right temporal lobe epilepsy. *AJNR Am J Neuroradiol* 2009;30:1740–1747.
4. Otte WM, van Eijsden P, Sander JW, et al. A meta-analysis of white matter changes in temporal lobe epilepsy as studied with diffusion tensor imaging. *Epilepsia* 2012;53:659–667.
5. Concha L, Kim H, Bernasconi A, et al. Spatial patterns of water diffusion along white matter tracts in temporal lobe epilepsy. *Neurology* 2012;79:455–462.
6. Winston GP. The potential role of novel diffusion imaging techniques in the understanding and treatment of epilepsy. *Quant Imaging Med Surg* 2015;5:279–287.
7. Pasternak O, Westin CF, Bouix S, et al. Excessive extracellular volume reveals a neurodegenerative pattern in schizophrenia onset. *J Neurosci* 2012;32:17365–17372.
8. McDonald CR, White NS, Farid N, et al. Recovery of white matter tracts in regions of peritumoral FLAIR hyperintensity with use of restriction spectrum imaging. *AJNR Am J Neuroradiol* 2013;34:1157–1163.
9. French JA. Imaging brain inflammation: if we can see it, maybe we can treat it. *Epilepsy Curr* 2016;16:24–26.
10. Lee CY, Tabesh A, Spampinato MV, et al. Diffusional kurtosis imaging reveals a distinctive pattern of microstructural alternations in idiopathic generalized epilepsy. *Acta Neurol Scand* 2014;130:148–155.
11. Bonilha L, Lee CY, Jensen JH, et al. Altered microstructure in temporal lobe epilepsy: a diffusional kurtosis imaging study. *AJNR Am J Neuroradiol* 2015;36:719–724.
12. Gao Y, Zhang Y, Wong CS, et al. Diffusion abnormalities in temporal lobes of children with temporal lobe epilepsy: a preliminary diffusional kurtosis imaging study and comparison with diffusion tensor imaging. *NMR Biomed* 2012;25:1369–1377.
13. Lemkaddem A, Daducci A, Kunz N, et al. Connectivity and tissue microstructural alterations in right and left temporal lobe epilepsy revealed by diffusion spectrum imaging. *Neuroimage Clin* 2014;5:349–358.
14. Jensen JH, Helpern JA, Ramani A, et al. Diffusional kurtosis imaging: the quantification of non-Gaussian water diffusion by means of magnetic resonance imaging. *Magn Reson Med* 2005;53:1432–1440.

15. White NS, Leergaard TB, D'Arceuil H, et al. Probing tissue microstructure with restriction spectrum imaging: histological and theoretical validation. *Hum Brain Mapp* 2013;34:327–346.
16. White NS, McDonald CR, Farid N, et al. Improved conspicuity and delineation of high-grade primary and metastatic brain tumors using "restriction spectrum imaging": quantitative comparison with high B-value DWI and ADC. *AJNR Am J Neuroradiol* 2013;34:958–964, S951.
17. McDonald CR, Delfanti RL, Krishnan AP, et al. Restriction spectrum imaging predicts response to bevacizumab in patients with high-grade glioma. *Neuro Oncol* 2016 pii: now063.
18. White NS, Dale AM. Optimal diffusion MRI acquisition for fiber orientation density estimation: an analytic approach. *Hum Brain Mapp* 2009;30:3696–3703.
19. White NS, Dale AM. Distinct effects of nuclear volume fraction and cell diameter on high b-value diffusion MRI contrast in tumors. *Magn Reson Med* 2014;72:1435–1443.
20. Holland D, Kuperman JM, Dale AM. Efficient correction of inhomogeneous static magnetic field-induced distortion in Echo Planar Imaging. *NeuroImage* 2010;50:175–183.
21. McDonald CR, Leyden KM, Hagler DJ, et al. White matter microstructure complements morphometry for predicting verbal memory in epilepsy. *Cortex* 2014;58:139–150.
22. White NS, McDonald C, Farid N, et al. Diffusion-weighted imaging in cancer: physical foundations and applications of restriction spectrum imaging. *Cancer Res* 2014;74:4638–4652.
23. Schwarz CG, Reid RI, Gunter JL, et al. Improved DTI registration allows voxel-based analysis that outperforms tract-based spatial statistics. *NeuroImage* 2014;94:65–78.
24. Avants BB, Tustison NJ, Song G, et al. A reproducible evaluation of ANTs similarity metric performance in brain image registration. *NeuroImage* 2011;54:2033–2044.
25. Tustison NJ, Avants BB, Cook PA, et al. Logical circularity in voxel-based analysis: normalization strategy may induce statistical bias. *Hum Brain Mapp* 2014;35:745–759.
26. Smith SM, Nichols TE. Threshold-free cluster enhancement: addressing problems of smoothing, threshold dependence and localisation in cluster inference. *NeuroImage* 2009;44:83–98.
27. Hagler DJ Jr, Ahmadi ME, Kuperman J, et al. Automated white-matter tractography using a probabilistic diffusion tensor atlas: application to temporal lobe epilepsy. *Hum Brain Mapp* 2009;30:1535–1547.
28. Bonilha L, Lee CY, Jensen JH, et al. Altered microstructure in temporal lobe epilepsy: a diffusional kurtosis imaging study. *AJNR Am J Neuroradiol* 2015;36:719–724.
29. Zhang Y, Yan X, Gao Y, et al. A preliminary study of epilepsy in children using diffusional kurtosis imaging. *Clin Neuroradiol* 2013;23:293–300.
30. Glenn GR, Jensen JH, Helpern JA, et al. Epilepsy-related cytoarchitectonic abnormalities along white matter pathways. *J Neurol Neurosurg Psychiatry* 2016;87:930–936.
31. Imamura H, Matsumoto R, Takaya S, et al. Network specific change in white matter integrity in mesial temporal lobe epilepsy. *Epilepsy Res* 2016;120:65–72.
32. Lee CY, Tabesh A, Benitez A, et al. Microstructural integrity of early- versus late-myelinating white matter tracts in medial temporal lobe epilepsy. *Epilepsia* 2013;54:1801–1809.
33. Concha L, Livy DJ, Beaulieu C, et al. In vivo diffusion tensor imaging and histopathology of the fimbria-fornix in temporal lobe epilepsy. *J Neurosci* 2010;30:996–1002.
34. Volmering E, Niehusmann P, Peeva V, et al. Neuropathological signs of inflammation correlate with mitochondrial DNA deletions in mesial temporal lobe epilepsy. *Acta Neuropathol* 2016;132:277–288.
35. Gershen LD, Zanotti-Fregonara P, Dustin IH, et al. Neuroinflammation in temporal lobe epilepsy measured using positron emission tomographic imaging of translocator protein. *JAMA Neurol* 2015;72:882–888.
36. Wang Y, Sun P, Wang Q, et al. Differentiation and quantification of inflammation, demyelination and axon injury or loss in multiple sclerosis. *Brain* 2015;138:1223–1238.
37. Wang X, Cusick MF, Wang Y, et al. Diffusion basis spectrum imaging detects and distinguishes coexisting subclinical inflammation, demyelination and axonal injury in experimental autoimmune encephalomyelitis mice. *NMR Biomed* 2014;27:843–852.
38. Zeineh MM, Holdsworth S, Skare S, et al. Challenges of high-resolution diffusion imaging of the human medial temporal lobe in Alzheimer disease. *Top Magn Reson Imaging* 2010;21:355–365.
39. Janz P, Savanthrapadian S, Haussler U, et al. Synaptic remodeling of entorhinal input contributes to an aberrant hippocampal network in temporal lobe epilepsy. *Cereb Cortex* 2016 pii: bhw093.
40. Concha L, Beaulieu C, Collins DL, et al. White-matter diffusion abnormalities in temporal-lobe epilepsy with and without mesial temporal sclerosis. *J Neurol Neurosurg Psychiatry* 2009;80:312–319.

Supporting Information

Additional Supporting Information may be found in the online version of this article:

Figure S1. Voxel-based group comparisons between patients with right TLE (RTLE) or left TLE (LTLE) and age-matched controls using ANTS registration.

Table S1. Mean volume fractions and standard deviations for IF, IH, MD, and CF for the controls and patients with TLE.

Table S2. Mean raw values and ranges for IF, IH, MD, and CF for the controls and patients with TLE.